ACS SENSORS

pubs.acs.org/acssensors

Article

Reflection-Enhanced Raman Identification of Single Bacterial Cells Patterned Using Capillary Assembly

Joong Bum Lee, Eojin Rho, Minjoon Kim, Sejoon Huh, Seoyoung Kim, Stefan A. Maier, Emiliano Cortés, Sungho Jo,* Yeon Sik Jung,* and Yoonsung Nam*

Cite This: *ACS Sens.* 2025, 10, 5908–5917

Read Online

ACCESS | Metrics & More | Article Recommendations | Supporting Information

ABSTRACT: Raman spectroscopy is an enticing tool for the rapid identification of pathogenic bacteria and has the potential to meet the demand for early diagnosis and timely treatment of patients. However, it remains a challenge to devise a reliable Raman detection platform to obtain reproducible signals from single bacterial cells. Herein, we utilize a reflective Ag/SiO_2 film that enhances the intrinsically weak Raman signals by re-excitation of the bacteria and reflection of downward-scattered photons, with maximum Raman intensities recorded by exciting the central edge of each single cell. The reflection-based configuration is simple, and its reliability as a sensing platform is validated by deep learning analysis. Importantly, given the positional dependence of the laser light on the Raman intensity, we employ capillarity-assisted particle assembly (CAPA) to selectively position single bacterial cells into a reflective topographical template to align the most Raman active region of the cell per the trap site geometry. Moreover, CAPA is utilized to directly isolate single cells from a suspension of artificial urine, eradicating any additional steps previously required to separate bacteria from biological samples. The proposed system has positive implications for future clinical settings that require simple, accurate, and reproducible detection of bacteria at the single-cell level.

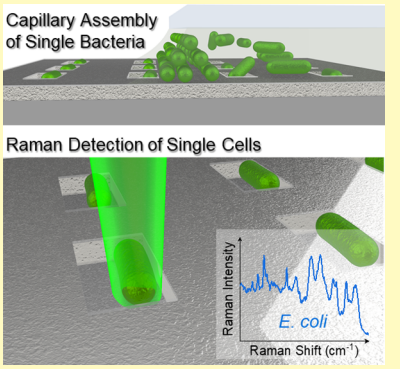

KEYWORDS: *single bacterial cells, Raman spectroscopy, deep learning, capillary assembly, patterning*

Bacterial infections and diseases caused by pathogenic microorganisms in food, water, and bodily fluids continue to stand as one of the major health threats affecting individuals worldwide each year. The impact is felt directly in various fields including clinical diagnostics, food and water safety, and environmental quality control.[1] Reliable and accurate detection of pathogenic bacteria is therefore crucially needed to meet the demands for early diagnosis and timely treatment of patients. Existing detection methods suffer from several limitations: poor differentiation of live and dead bacteria for polymerase chain reaction (PCR),[2] limited sensitivity and cross-reactions of antigens for enzyme-linked immunosorbent assay (ELISA),[3] and the need for trained personnel for flow cytometry.[4] The search for and development of techniques that satiate the ideal requirements of fast data acquisition, high sensitivity, specificity, and direct detection is, therefore, an actively ongoing process.

In light of this, several methods have emerged to this end including lateral flow immunoassay,[5] matrix-assisted laser desorption/ionization time-of-flight mass spectroscopy,[6] electrochemical impedance spectroscopy,[7] and holographic imaging.[8] Particularly, Raman spectroscopy has received much attention over the years as an optical technique that offers the advantages of rapid and direct detection of bacteria, with its molecular fingerprint information as the final signal output.[9,10] Several studies have utilized surface-enhanced Raman spectroscopy (SERS) as a means to enhance the inherently weak Raman signals, either by decorating the bacteria surface with metal nanoparticles[11−16] or placing bacterial cells on top of nanostructured metallic substrates.[17−20] Amidst the growing interest in SERS of bacteria, there are still open challenges that remain in detecting bacteria at the single-cell level. One notable challenge is to obtain highly reproducible and accurate fingerprint signals. As overall signal intensities from single cells are typically an order of magnitude smaller than those of bulk samples,[21] signal reliability and reproducibility take priority in accurately detecting and identifying single bacterial species. In this aspect, it is still debatable whether SERS is the ideal method to enhance the Raman signals from bacteria because of the difficulty to achieve uniform signals arising from polydispersity and uneven distribution of nanostructures that interact with the bacterial surface.[22,23] Another challenge arises in rapidly obtaining the highest signal intensity from individual cells. A vast majority of reported methods involve drop-casting and drying bacterial suspensions on substrates, which requires

Received: April 12, 2025
Revised: July 18, 2025
Accepted: July 21, 2025
Published: August 4, 2025

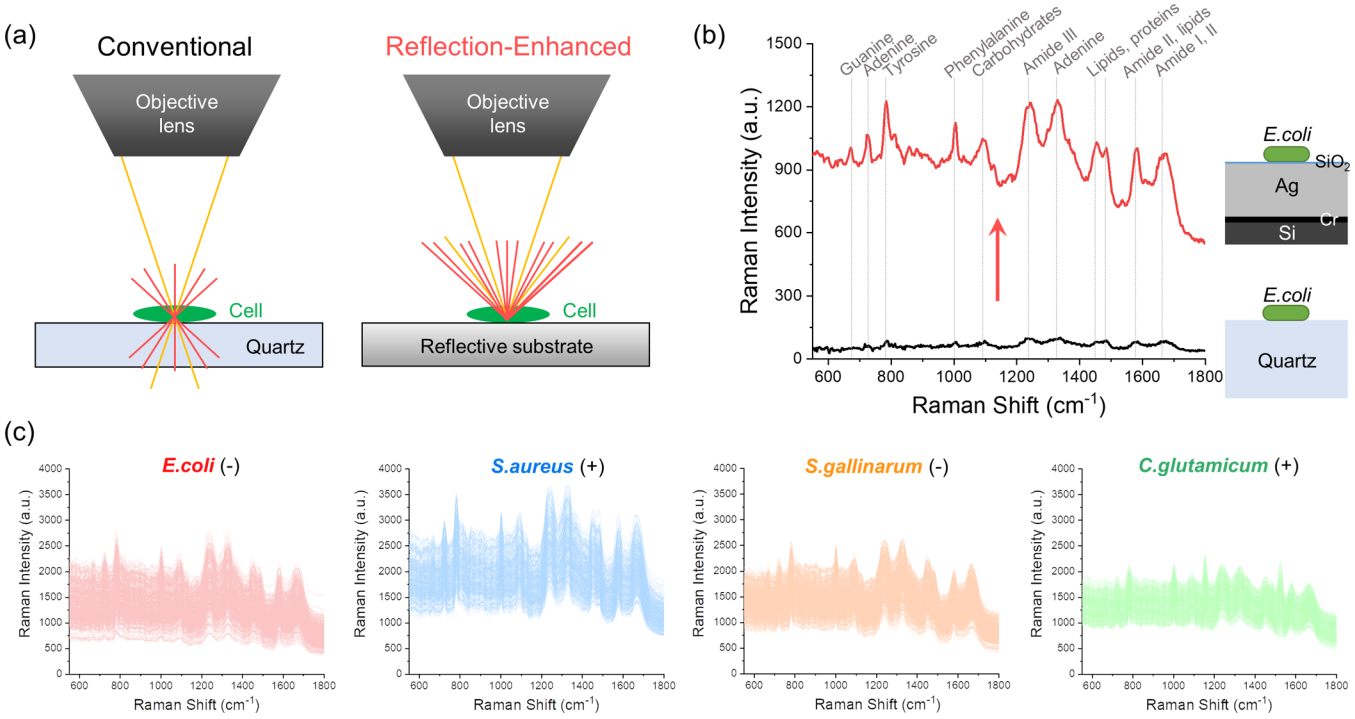

Figure 1. Reflection-enhanced Raman spectroscopy. (a) Illustration of the working principle. Signal enhancement arises from the reflection of the laser light for re-excitation of the bacterial cell and reflection of the downward scattered Raman photons back toward the detector. (b) Characteristic Raman spectra of *E. coli* taken from conventional quartz (black) and reflective Ag/SiO_2 (red) substrates. (c) Highly reproducible signals for *E. coli*, *S. aureus*, *S. gallinarum*, and *C. glutamicum*. Plots represent raw spectra taken from 260 individual cells per species.

navigation through the sample to find and select single cells for measurement. As signal intensities vary depending on the position of the excitation laser beam on the bacteria, the deterministic orientation of cells is highly desirable to rapidly obtain the highest intensity profiles.

In this work, we utilize a reflection-based Raman signal enhancement strategy combined with capillarity-assisted particle assembly (CAPA) to detect single bacterial cells, aiming to achieve high signal reproducibility, detection efficiency, and simplicity. To obtain sufficient intensities of fingerprint information, Raman signals are enhanced using a highly reflective mirror by the reflection of downward scattered Raman photons and the back reflection of the incident laser beam, both of which would be absent in the case of a transparent substrate.[24] The reliability of the reflection-based strategy is validated using deep learning and machine learning techniques to quantify the classification accuracies of different bacterial species. Importantly, provided the positional influence of the excitation laser on the Raman signal intensities arising from the bacteria, CAPA is employed to position single cells in a deterministic manner to regularly align their most Raman active regions. CAPA, which uses capillary forces to trap single or multiple colloidal particles into predefined topographic templates,[25−28] has emerged to be a useful tool over other colloidal patterning techniques[29,30] when discrete and accurate positioning of single particles is necessary. Moreover, a notable advantage over methods such as optical printing[31,32] and electrophoretic deposition[33,34] is that particles are free of damage as there are no external stimuli (e.g., high-power lasers or voltages) acting upon the particles. Previous reports have indeed shown that CAPA is highly compatible with biological samples, as demonstrated with the patterning of DNA molecules,[35,36] phospholipids,[37] and cells.[38,39] This work provides the first demonstration of using CAPA to selectively isolate bacteria at the single-cell level for the purpose of Raman identification. Finally, the isolation capacity of CAPA is capitalized to pattern and obtain Raman spectra from single cells not only in the form of purified suspensions but also of artificial urine, meeting the demand for minimal sample preparation and purification steps.

RESULTS AND DISCUSSION

Reflection-Enhanced Raman Spectroscopy. The Raman enhancement strategy in this study is based on the use of highly reflective substrates (Figure 1a). In conventional Raman spectroscopy, a transparent substrate, such as CaF_2 or quartz, is used to minimize background signals that potentially overlap with the characteristic spectra of the sample.[40] The excitation of the sample by the laser occurs only once, and only those Raman photons directed back toward the objective lens are recorded into the detector. In contrast, signals from a sample drop-casted and supported by a reflective film substrate can be enhanced by the reflection of downward scattered Raman photons and the reflection of the laser itself for re-excitation of the sample, with each of the two events effectively doubling the signal intensities.[24,41] From Figure 1b, the enhancement effect is evident by comparing the Raman signature spectra of a single *E. coli* cell placed on a reflective Ag/SiO_2 substrate to a quartz substrate. Despite the difference in the signal intensities, both Raman spectra exhibit matching peaks that can be readily assigned to the various components of bacteria (e.g., DNA, lipids, carbohydrates) as reported in literature.[42] To ensure the highest possible Raman intensities, several experimental parameters had to be carefully considered.

First, the choice of reflective material was based on the materials' reflectance across the visible window that includes

https://doi.org/10.1021/acssensors.5c01225
ACS Sens. 2025, 10, 5908−5917

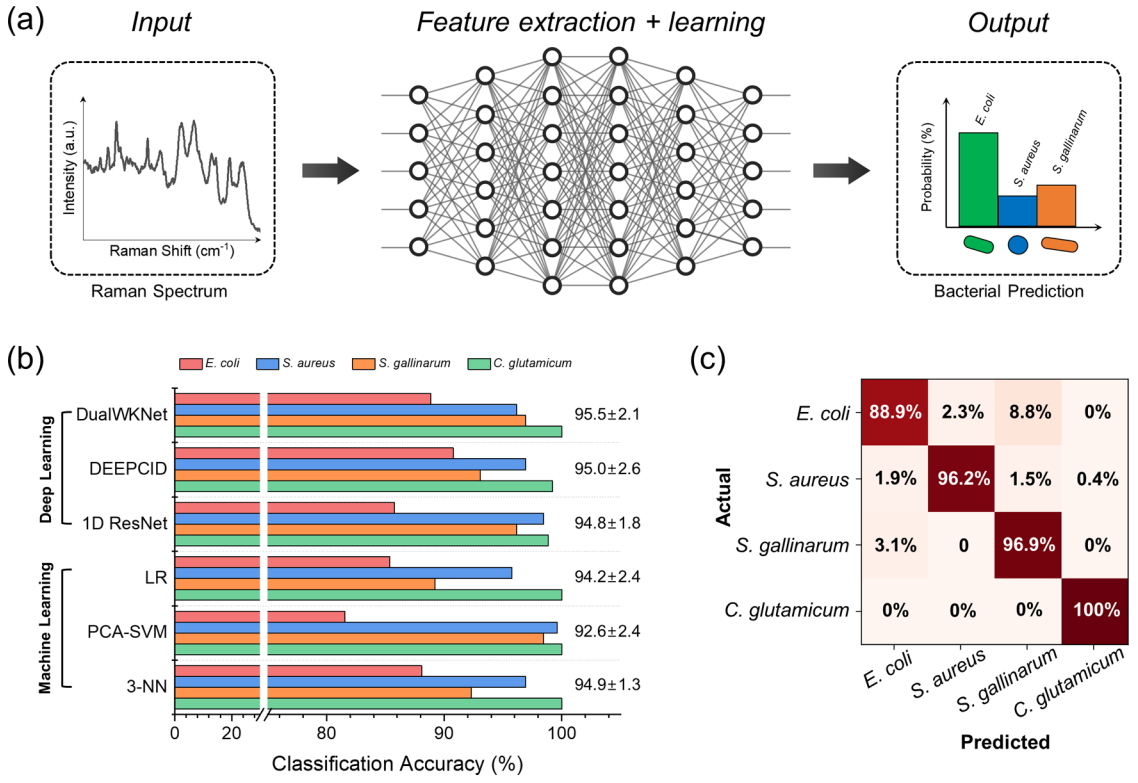

Figure 2. Bacteria classification using deep learning. (a) General deep learning process for bacterial classification using Raman spectra. (b) Classification accuracy of the four different bacterial species using various deep learning and classical machine learning models. (c) Confusion matrix formulated using DeepWKNet as the representative model based on the highest average classification accuracy.

the excitation wavelengths and the inherent background signal from the material. Three commonly used reflective materials—Ag, Au, and Al—were thus compared experimentally to assess their optical reflectance properties and spectral background characteristics under identical acquisition settings. For normal incidence as in the case of the current spectroscopic setup, reflectance is directly governed by refractive index n and extinction coefficient k (more details in Supplementary Note 1). Among the three metals, Ag has the highest reflectance values throughout the visible spectrum and the lowest intrinsic background signal (Figure S1). The advantage of the latter is exemplified by the fact that no signal processing is needed to directly visualize and assign the characteristic peaks that correspond to the bacteria at hand. It should be noted that for Ag, a thin layer of SiO_2 was additionally deposited (hence labeled Ag/SiO_2) to protect the bacterial cells from antibacterial rupture.[42] While Au and Al were tested without SiO_2 passivation, this comparison was intended to benchmark optical trends rather than establish mechanistic equivalence, and Ag/SiO_2 was selected as the primary sensing platform for all measurements in the study. Another important parameter in optimizing signal intensities was the bacteria washing process. Because bacteria are typically grown in nutrient media which comprise multiple ingredients, it is vital to remove the media to obtain the fingerprint information on only the bacteria. While typical washing processes comprise three to five repeated centrifugation and suspension of pellets in deionized water,[17,43,44] the use of deionized water during all washing cycles can easily expose the cells to osmotic shock due to a sudden difference in salt concentrations. The effect is detrimental because the low osmotic pressure leads to water entering the cell, increasing its internal pressure, and eventually causing lysis.[42] To prevent osmotic shock during the washing processes the first three washes were conducted using an isotonic solution (0.9% NaCl) followed by one last wash with deionized water (Figure S2a). From Figure S2b, the morphology of cells is different as seen by the smaller overall size and better contrast in the contour of the cell. The improved signal intensities highlight the importance of maintaining cell morphology during the washing process. Finally, the most important factor for signal optimization was the position of the excitation laser on the bacterial cell. Given that the Raman spectrometer records back-reflected signals (Figure S3a), it was presumed that the highest signal intensities from each bacterial cell would arise when the laser beam is focused at the edge of the cell where photons can be readily back-reflected. This was indeed the case when measuring across different parts of the bacteria (Figure S3b). Intriguingly, the opposite edge of the most active part of the cell exhibits very limited signals (marked by the cyan blue dot), suggesting a possible asymmetry in the spatial distribution or density of Raman-active molecular components at different sides of the bacterial envelope.[45,46] In consideration of such various parameters, the reflection-enhancement configuration enabled highly reproducible signals to be obtained from single-cell measurements for different pathogenic bacteria namely *Escherichia coli*, *Staphylococcus aureus*, and *Salmonella gallinarum*, as well as a nonpathogenic *Corynebacterium glutamicum* (Figure 1c). The Raman profiles from each bacterial species represent raw spectra from 260 different single cells.

With highly repeatable signals at hand using the reflective substrate, single bacteria measurements were also made on a nanostructured Ag substrate (Figure S4a) to affirm the lack of reproducibility of SERS for the bacteria identification. First, to

https://doi.org/10.1021/acssensors.5c01225
ACS Sens. 2025, 10, 5908−5917

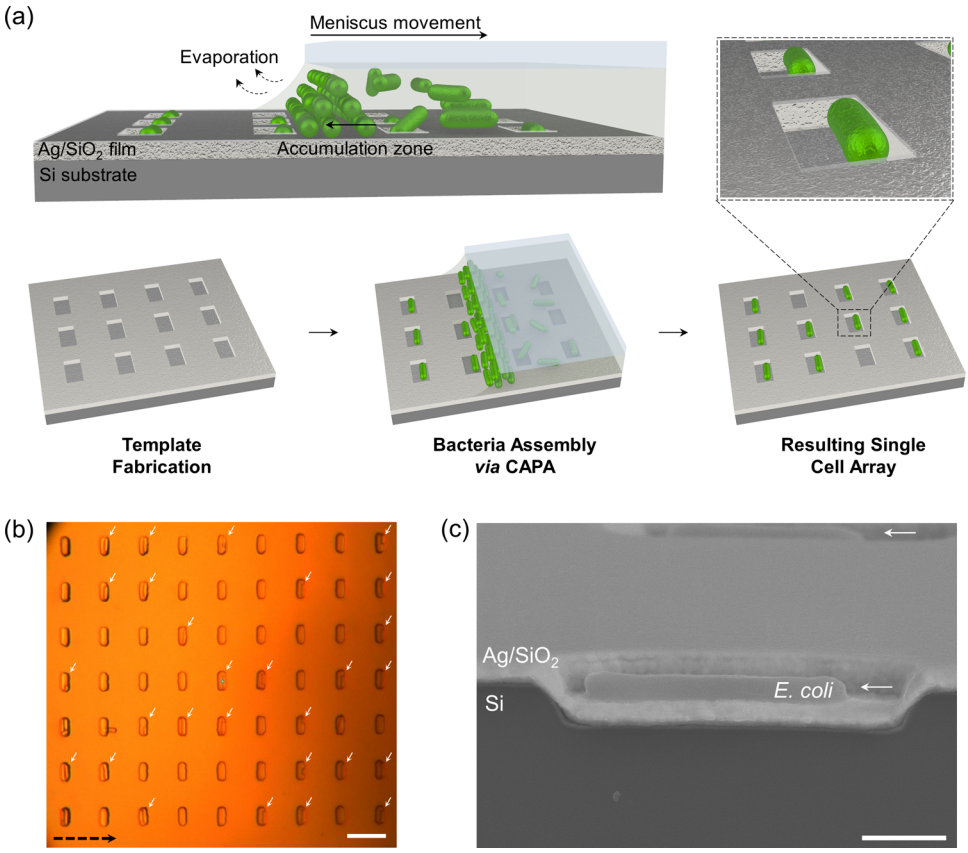

Figure 3. CAPA of single bacterial cells. (a) Schematic illustration of the CAPA process. (b) Bright-field image of single *E. coli* cells positioned within the patterned traps. Scale bar: 10 μm. (c) Cross-sectional SEM image of a single cell inside a trap. Scale bar: 1 μm.

ratify that the substrate itself is befitting for SERS, a Rhodamine B solution was drop-casted on the nanostructured Ag substrate to give highly reproducible characteristic SERS signals across 30 random spots (Figure S4b).[47,48] However, when the SERS response was recorded for 25 different single *E. coli* cells using the same substrate (Figure S4c), the variability of spectra both in peak positions and peak intensities is high across the entire sample set, making it difficult to assign peaks that represent the signature signals of bacteria. The issue of reproducibility was further verified by measuring the SERS response of Ag nanoparticle-decorated *E. coli* (Figure S5), which exhibit similar variations. The SERS results suggest that, unlike the case of probing small molecules like Rhodamine B, it is difficult to obtain uniform signals with specimens substantially greater in size than the electromagnetic hotspots. For micron-scale biological entities such as bacteria, the viscoelastic nature of cells and cell-to-cell variation in both shapes and sizes are unavoidable setbacks that make it difficult to achieve signal uniformity.[49]

Deep Learning for Bacteria Classification. Having established a reproducible set of data, the reliability of the reflection-based detection platform was assessed by quantifying the identification accuracy of each bacterial species via deep learning analysis. Deep learning is an artificial intelligence technique that enables hierarchical feature extraction based on multiple layers of trainable parameters and has been actively used in computer vision tasks.[50−52] In recent years, the use has expanded to processing Raman spectral data for bacteria identification.[53−57] The general process for deep learning is given in Figure 2a, where feature extraction and learning of features from the input spectra are used to ultimately return the probability of bacterial prediction. For the four bacterial species, multiple reported deep learning models were implemented to quantify their identification accuracy, namely one-dimensional residual network architecture (1D ResNet),[54] deep learning-based component identification,[53] and the recently reported dual-branch wide kernel network (Dual-WKNet).[55] Figure 2b shows the accuracy results for the different models as well as those for conventional machine learning methods including 3-nearest neighbor (3-NN), support vector machine with principal component analysis (PCA-SVM), and logistic regression (LR). The returned identification accuracies are high throughout all techniques (>92% on average), which helps validate the reliability of reflection-enhanced Raman as a means to obtain Raman signals of high reproducibility. The highest average accuracy was returned by the DualWKNet model (configuration shown in Figure S6), which is based on accurate training of global spectral features even with few training data owing to wide kernels (large kernel sizes, >15) for large receptive fields and minimized overfitting.[55] To further examine the identification accuracies for each bacterial species, a confusion matrix was plotted in Figure 2c using DualWKNet as the representative model. The accuracies as indicated by the red diagonal sections were measured using a 5-fold cross-validation process (a percentage out of 260 spectra), showing satisfactory results for each bacterial class. Overall, the high classification accuracy provided by DualWKNet alongside other machine and deep learning models serves as a validation of reflection-enhanced

https://doi.org/10.1021/acssensors.5c01225
ACS Sens. 2025, 10, 5908−5917

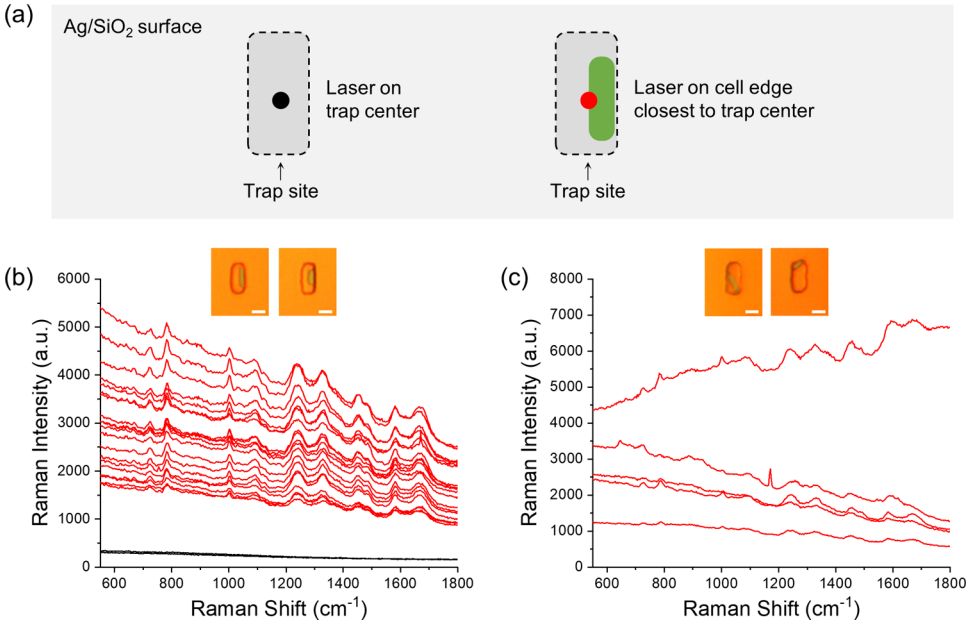

Figure 4. Raman signals from single cells isolated using CAPA. (a) Top-view illustration of a single *E. coli* cell inside the trap site (in dashed lines) and the positions of the excitation laser colored to match the Raman spectra in panel (b). Raman spectra of single *E. coli* cells entrapped using CAPA (b) and by drop-casting on patterned templates (c). Two examples of single cells positioned within traps by CAPA and by drop-casting show the difference in orientation of the cells. Each single bacterial cell is color-coded in light green. Scale bars: 2 μm.

Raman as a means to provide highly reliable signature signals from bacteria.

CAPA of Single *E. coli* Cells. As demonstrated previously in Figure 1, Raman detection of single bacteria typically involves drop-casting a small volume of bacterial suspension on a given substrate and then navigating through the sample to find single cells for measurement. So far, it has been necessary to excite different parts of the cell to find the region of highest Raman activity (central edge of the cell as provided in Figure S3) for an accurate and judicious comparison of the signature spectra of different bacteria. However, the random orientation of drop-casted cells makes each consecutive single-cell measurement increasingly laborious in obtaining the highest signal intensities. To alleviate this issue, it would be ideal to position individual cells with a unified orientation. We thus employed CAPA, a patterning technique that uses capillary forces to trap colloids at predefined topographical sites.[25,27,58]

Figure 3a shows the schematic illustration of using CAPA to assemble *E. coli* into an array of single cells. After fabricating the assembly template as per Figure S7, the bacterial suspension was confined between the template and a glass slide that moves across to form a receding meniscus. The solvent evaporation at the meniscus creates a flux that promotes the convective flow of cells toward the meniscus edge, generating an accumulation zone (AZ) at the three-phase (solid template/bacterial suspension/vapor) contact line.[25] The AZ at the edge of the meniscus restricts the Brownian motion of cells in suspension and hence increases the probability of successful assembly. The cells are forced into the designated traps as the moving meniscus locally pins as it encounters the patterned trenches.[27] After translation of the suspension across the template is complete, an array of single bacterial cells is obtained, with each cell indicated by white arrows (Figure 3b). As the assembly direction is from left to right, the cells are positioned at the righthand side of the trap. The SEM image in Figure 3c confirms the localization of one cell per trap. We note that while assembly yields can be improved by multiple runs of CAPA as noted previously in patterning of cells,[38] a single run was conducted to minimize preparation time and was sufficient to find multiple single cells entrapped for Raman detection, as observed by optical microscopy. Thus, having created an alignment of single cells according to the trap geometry, the Raman spectra of the patterned cells were obtained next.

Figure 4a illustrates the position of the excitation laser that corresponds to the Raman spectra of single *E. coli* cells patterned using CAPA (in red, Figure 4b) and an empty trap (in black, Figure 4b). The reflection-enhanced Raman response from the patterned cells is consistent with those from cells drop-casted on the Ag/SiO_2 substrate, indicated by the precisely matching peaks of spectra that arise from the Raman and reflection-enhanced Raman effects (and not SERS), shown in Figure S8. For measuring the patterned cells, the laser was consistently focused on the central edge of the cell closest to the trap center. The result in Figure 4b highlights the importance of CAPA in providing an alignment of single cells. It is worth noting that even though the laser was positioned at the same location—centered on the trap—we consistently observed stronger Raman signals from CAPA-aligned bacteria. We hypothesize that this may result from anisotropic drying effects and preferential bacterial orientation or enhanced contact of one side with the trap cavity. While the exact mechanism remains under investigation, these findings suggest that CAPA may enable spontaneous alignment of the signal-dominant side of the bacterium in a reproducible manner. We aim to explore this further in future studies using high-resolution Raman mapping and modeling of capillary flow dynamics. Because positioning the laser at the central edge of the bacteria is imperative to acquire the highest signal intensities, the use of CAPA makes the laser positioning and spectral acquisition processes significantly more convenient. This, for instance, cannot be achieved with drop-casting

https://doi.org/10.1021/acssensors.5c01225
ACS Sens. 2025, 10, 5908−5917

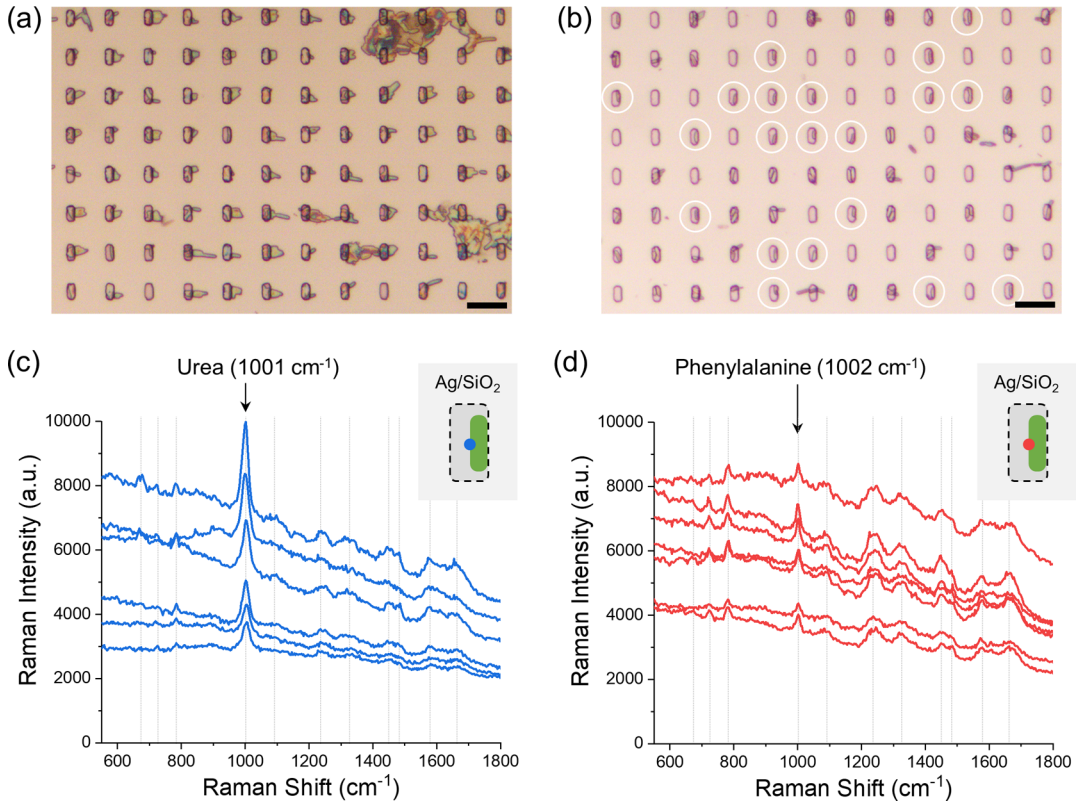

Figure 5. CAPA-enabled separation of single bacterial cells directly from artificial urine. Bright-field images of CAPA conducted for *E. coli* in a suspension of artificial urine before (a) and after (b) rinsing the substrate with deionized water. Single cells trapped successfully in (b) are indicated by white circles. Scale bars: 10 μm. (c) and (d) Single-cell Raman spectra taken from panels (a) and (b), respectively.

because each cell would have a different orientation on the substrate (Figure 4c). Additionally, the fixed orientation of cells enabled via CAPA brings about consistency in the spectra obtained. When cells were drop-casted on the patterned substrate for comparison, with all other measurement conditions kept identical, the general trend of the characteristic spectra was notably irregular. The discrepancy is likely to come from a difference in the local orientation of each cell within the trap site from the two samples, with CAPA providing the benefit of pinning the cells adjacent to the trap wall for regularity in alignment. While the current demonstration focused on rod-shaped *E. coli* and rectangular trap geometry to emphasize the aligning capability of CAPA, the technique can be extended to assembling mixed bacteria with different cell shapes in future studies by rational design of the template with different patterns[59] to accommodate the cells' structural variety. In addition, using artificial intelligence algorithms for the recognition of bacterial cells different morphologies can help determine the optimal position for laser excitation and thus streamline the Raman spectral acquisition process.

Separation of Single *E. coli* Cells From Artificial Urine. Given the working principle of CAPA in that the suspension of bacterial cells is swept across the topographical template, the separation capability of CAPA was explored to determine whether *E. coli* cells suspended in media other than deionized water can be selectively filtered at the trap sites. As a proof-of-concept, CAPA was conducted for *E. coli* cells suspended in artificial urine, with Figure 5a showing the results of assembly directly after CAPA. Here, the traps appear to be occupied but not discretely within the trap boundaries. To remove any components hanging out from the righthand ends of the traps, a simple rinsing process was carried out, resulting in a clearer representation of trapped cells, as shown in Figure 5b. Again, the cells positioned adjacent to the righthand side of the trap are the ones properly assembled using the CAPA process, and these cells have been marked with white circles. The results for artificial urine are in stark contrast with those for other media (ground beef solution, LB media, milk, and whole blood from mouse) given in Figure S9. In all other cases, no cells were observed to be trapped both after CAPA and after the rinsing process. As CAPA is fundamentally based on evaporation of the receding suspension, the presence of multiple components in these various media interferes with the formation of a dense accumulation zone of the bacterial cells which, in turn, prevents the capillary forces to come into play at the local trap sites. Provided the separation capability of CAPA for artificial urine, Raman measurements were conducted to determine whether the signature *E. coli* signals can be readily obtained from cells before and after the rinsing process.

Figure 5c shows the characteristic Raman signals of *E. coli* for cells measured directly after CAPA, with characteristic peaks indicated by gray lines. A clear difference in the spectra is observed before and after the rinsing process. In Figure 5c, a high-intensity peak that pertains to urea is present at 1001 cm^{-1}, which overlaps with the phenylalanine peak at 1002 cm^{-1} shown in Figure 5d. The urea peak is removed after the rinsing process, and it is also evident that overall consistency and peak intensities are higher for the water-rinsed samples due to the removal of the remnants. The result indicates the potential to utilize CAPA in detecting bacteria suspended in biological samples from patients with urinary tract infections.[60,61] With bacterial cells already present in urine, CAPA

https://doi.org/10.1021/acssensors.5c01225
ACS Sens. 2025, 10, 5908−5917

can help omit any further processing steps such as centrifugation, as cells can be selectively trapped into designated sites to be detected directly using Raman spectroscopy.

CONCLUSIONS

In this work, a single bacteria detection platform was introduced in which single cells are selectively patterned using CAPA and characterized using reflection-enhanced Raman spectroscopy. To obtain reliable signals with high reproducibility, special attention was given to establishing the reflective film with a low background signal, the bacteria washing processes to maintain cell morphology, and the measurement conditions especially the position of the excitation laser. The highly reflective Ag/SiO_2 film, which enhances signals by the reflection of downward scattered Raman photons and the excitation laser, enabled the detection of different bacterial species. The excellent reproducibility of the reflection-based substrate was validated by both previously reported machine and deep learning techniques. The role of CAPA is significant in that it enables the orientation of the bacterial cells according to the geometry of the patterned traps which, in turn, align the part of the cell that provides the highest signal intensity. Another important benefit of CAPA is its separation capability in selectively isolating single cells from an *E. coli* suspension in artificial urine. Raman detection of entrapped cells directly from the urine suspension has positive implications for applications involving biological samples as no additional processing steps such as centrifugation is required. While the simple reflection-based platform coupled with CAPA offers a step toward reliable, accurate, and reproducible detection of pathogenic bacteria at the single-cell level, there are a number of aspects that could be further improved. First, the lengthy patterning process governed by the assembly speed of 2 μm s^{-1} needs to be shortened. For instance, this could be achieved by utilizing a patterned blade to drag the bacterial suspension, increasing the evaporation rate of the meniscus.[62] Higher evaporation rates leading to increased cell flux to the meniscus edge can, in parallel, provide the added potential benefit of reducing the minimum bacterial concentration needed for cell capture. We anticipate that making this engineering adjustment can help make the platform more compatible with lower bacterial densities present in real urine samples. Additionally, the data set could be expanded to encompass several other bacterial species to fully harness the synergistic potential of integrating Raman spectroscopy and deep learning. We envision that these improvements could help push the proposed system to achieve greater practical relevance.

EXPERIMENTAL SECTION

Growth of Bacteria. Bacterial suspensions were prepared by thawing and inserting a small piece of frozen bacteria stock (stored at −75 °C) into 7 mL of growth media (Luria Broth for *E. coli* and Brain Heart Infusion for *C. glutamicum*, *S. gallinarum*, and *S. aureus*) and incubating overnight with aeration at 37 °C. A volume of 50 μL overnight grown solution was added to 7 mL of fresh media and grown under identical conditions until an O.D. of around 0.3 was reached.

Washing of Bacterial Suspension. Bacterial suspensions were added to 1 mL tubes for a four-step washing process. Three initial washes were conducted by centrifuging the bacteria at 1000 *g* (for *E. coli* and *S. gallinarum*) or 6000 *g* (for *S. aureus*) and resuspending the pellets in 0.9% NaCl. In the final washing step, the pellets were resuspended in deionized water. The use of the isotonic solution in the early washing processes is to minimize osmotic shock during the removal of the growth media.

Preparation of Reflective Film Substrates. Reflective film substrates were prepared using electron beam evaporation (A-TECH, Republic of Korea). First, silicon wafers were diced into 1.5 cm × 1.5 cm pieces and sonicated sequentially in acetone, ethanol, and deionized water for 10 min each and then dried with N_2 gas. To remove excess contaminants, the substrates were O_2 plasma-treated for 2 min before electron beam deposition. Cr adhesion layers were deposited at a rate of 0.5 Å s^{-1} while reflective films, Ag, Au, and Al were all deposited at 2.0 Å s^{-1}. For Ag, a protective SiO_2 layer was additionally deposited at 0.1 Å s^{-1}.

Deep Learning Analysis Using DualWKNet. The DualWKNet model was previously developed to accurately discriminate different bacterial species based on their Raman spectra.[54] The model consists of two distinct network branches, each consisting of three sets of residual blocks and average pooling layers, and finally a self-attention block. The residual blocks discern features from the input spectra by employing convolution layers to act as trainable filters. The number of kernels in the convolution layers is identical (32, 64, and 128) in both network branches but the layers in each branch have different kernel sizes of 45, 25, and 15 for the first branch and 95, 55, and 15 for the second branch. After each residual block, the average pooling layer reduces the number of learning parameters and prevents overfitting. The following self-attention block then learns the correlations between the extracted spectral features. Finally, the fully connected layer returns the probability of each bacterial species for identification with the Softmax function applied as a classifier. The model was written in the Python language and adapted to the PyTorch deep learning framework.[63] Deep learning training was conducted through the AdamW[64] optimizer, with a learning rate of 7 × 10^{-5} and betas (0.5, 0.999). The batch size was 20, and 20 epochs were used. Every 5 epoch, the learning rate was halved. A Titan V (NVIDIA, USA) GPU was used to perform the DualWKNet model training.

Deep Learning Analysis Using DeepCID and 1-D ResNet. DeepCID is a model presented for distinguishing the composition of chemical mixtures from Raman spectra. The code for this model is publicly available at (https:github.com/xiaqiong/DeepCID), and in this study, we have reproduced the model using the PyTorch toolkit. The DeepCID model consists of multiple convolutional layers designed to capture the intricate patterns within the Raman spectra. The model features two convolutional blocks and a max-pooling block, with the first convolutional block having an output channel size of 32, and the second convolutional block having an output channel size of 64. The kernel size for all convolutional blocks is fixed at 5. Following feature extraction by the convolutional blocks, the extracted features pass through a fully connected layer for classification. The Rectified Linear Unit (ReLU) was used as the activation function, and training was conducted using the Adam optimizer with a learning rate of 0.0001.

The 1-D ResNet is a model presented for distinguishing bacterial spectra from Raman spectra. The code for this model is publicly available at (https://github.com/csho33/bacteria-ID). In our study, we reproduced the model and training techniques presented in the original publication on 1-D ResNet.[54] The proposed 1-D ResNet model is based on the widely used ResNet[51] model for image classification, which utilizes 2D convolutional blocks to analyze image data. However, in 1-D ResNet, 2D convolutional blocks are substituted with 1D convolutional blocks. The 1-D ResNet used in this work comprises several residual blocks, each consisting of two convolutional blocks with a kernel size of 5 and batch normalization. A total of 12 residual blocks are utilized, followed by feature extraction and classification through a subsequent fully connected layer. The ReLU was used as the activation function, and training was conducted using the Adam optimizer with a learning rate of 0.001.

Fabrication of the Assembly Template for CAPA. The first step to fabricating the assembly template is to undergo an image reversal process in standard photolithography. AZ5214E photoresist (Microchemicals GmbH, Germany) was spin-coated at 5000 rpm for

https://doi.org/10.1021/acssensors.5c01225
ACS Sens. 2025, 10, 5908−5917

30 s on a freshly cleaned Si substrate and prebaked at 115 °C for 1 min. Using the photomask designed to fit single bacterial cells, the resist was exposed to UV light (365 nm, 210 mJ cm^{-2}) for 5 s using an MDA-600S mask aligner (Midas System Co., Republic of Korea). The exposed photoresist was reversal baked at 115 °C for 2 min and subsequently flood-exposed without the photomask for 30 s. The resist was developed using an AZ MIF300 Developer (Merck KGaA, Germany) for 22 s and immediately rinsed with deionized water for 30 s. Reactive ion etching was used to create traps through the Si template using the patterned photoresist as the etching mask. A total of 14 cycles of SF_6 (80 W source power, 20 s) and C_4F_8 (80 W source power, 30 s) were used. The photoresist was then removed by sonication in acetone for 30 min. The reflective substrate was prepared by electron beam evaporation to deposit 30 nm Cr (adhesion layer), 300 nm Ag (reflective layer), and 1 nm SiO_2 (passivation layer) at rates of 0.5, 2.0, and 0.1 Å s^{-1}, respectively. For Ag, a thickness of 300 nm ensures that all sidewalls of the patterned traps are covered to prevent the Raman peak of Si (~520 cm^{-1}) from interfering with the characteristic Raman signals of bacterial cells. Additionally, the SiO_2 layer acts as a passivating layer to protect the bacteria from antibacterial rupture.[42]

Capillarity-Assisted Particle Assembly. CAPA was conducted using a customized setup. The assembly template was fixed on a metal block fixed over a hot plate set 25 °C above the dew point temperature. Around 150 μL of bacterial suspension was sandwiched between the template and a freshly cleaned glass coverslip. The bacterial suspension was prepared at O.D. values around 0.3, corresponding to volume fractions of approximately 0.000038%. This is a conservative concentration compared to a previous study on CAPA-based bacteria patterning,[39] chosen intentionally to reduce the probability of multibacterial occupancy while maintaining viable, exponentially growing cells. The coverslip was set to relative motion at a constant speed of 2 μm s^{-1} using a piezoelectric motor. Given the patterned area of 5 × 5 mm, the time taken to prepare one sample using the CAPA process is approximately 42 min.

Raman Measurements. A dispersive Raman spectrometer (ARAMIS, Horiba Jobin Yvon, France) equipped with 514, 633, and 785 nm lasers was used for Raman measurements. Based on experimental comparison, 514 nm was chosen as the excitation wavelength, and a grating of 600 grooves mm^{-1} was used to collect the Raman spectra of single bacteria cells. The resolution provided by the selected grating is approximately 2.8 cm^{-1}. The power and integration time were set to 1.25 mW and 10 s with no accumulations.

Bacterial Suspensions in Various Media for CAPA. To determine the separation capability of CAPA in selectively isolating bacteria from different media, milk (used as is from a commercial product), artificial urine (from Pickering Laboratories, USA), ground beef solution (prepared from a commercial product), LB media (prepared using LB powder purchased from Duchefa Biochemie, The Netherlands), and whole blood (heart blood from mouse) were used in the final washing step for resuspending *E. coli* cells. The following dilutions in deionized water were made to conduct CAPA: 50 times for milk, 10 times for artificial urine, and 100 times for whole blood. The use of deionized water for dilution was intended for direct comparison with medium-grown bacteria suspensions (washed with 0.9% NaCl three times and one final time with deionized water). As CAPA relies on controlled meniscus evaporation, the presence of salts or buffers such as PBS or 0.9% NaCl leads to salt crystallization at the drying front, interfering with the capillary flow and particle access to the microcavities. Hence, deionized water was selected as the dilution medium for CAPA compatibility.

■ ASSOCIATED CONTENT

Supporting Information

The Supporting Information is available free of charge at https://pubs.acs.org/doi/10.1021/acssensors.5c01225.

Supplementary notes (Notes 1 and 2) on reflectance and signal enhancement mechanism; supporting figures (Figures S1−S9) on selection of material and excitation laser, bacteria washing process, laser position, SERS from alternative systems, deep learning model configuration, patterned template fabrication, comparison of Raman and SERS, and suspension of *E. coli* in various media (PDF)

■ AUTHOR INFORMATION

Corresponding Authors

Sungho Jo − *School of Computing, Korea Advanced Institute of Science and Technology, Daejeon 34141, Republic of Korea*; Email: shjo@kaist.ac.kr

Yeon Sik Jung − *Department of Materials Science and Engineering, Korea Advanced Institute of Science and Technology, Daejeon 34141, Republic of Korea*; orcid.org/0000-0002-7709-8347; Email: ysjung@kaist.ac.kr

Yoonsung Nam − *Department of Materials Science and Engineering, Korea Advanced Institute of Science and Technology, Daejeon 34141, Republic of Korea; Department of Biological Sciences, Korea Advanced Institute of Science and Technology, Daejeon 34141, Republic of Korea*; orcid.org/0000-0002-7302-6928; Email: yoonsung@kaist.ac.kr

Authors

Joong Bum Lee − *Department of Materials Science and Engineering, Korea Advanced Institute of Science and Technology, Daejeon 34141, Republic of Korea*

Eojin Rho − *School of Computing, Korea Advanced Institute of Science and Technology, Daejeon 34141, Republic of Korea*

Minjoon Kim − *Department of Materials Science and Engineering, Korea Advanced Institute of Science and Technology, Daejeon 34141, Republic of Korea*

Sejoon Huh − *School of Computing, Korea Advanced Institute of Science and Technology, Daejeon 34141, Republic of Korea*

Seoyoung Kim − *Department of Materials Science and Engineering, Korea Advanced Institute of Science and Technology, Daejeon 34141, Republic of Korea*

Stefan A. Maier − *School of Physics and Astronomy, Monash University, Clayton, Victoria 3800, Australia; The Blackett Laboratory, Department of Physics, Imperial College London, London SW7 2AZ, U.K.*; orcid.org/0000-0001-9704-7902

Emiliano Cortés − *Chair in Hybrid Nanosystems, Nanoinstitute Munich, Faculty of Physics, Ludwig-Maximilians-Universität München, München 80539, Germany*; orcid.org/0000-0001-8248-4165

Complete contact information is available at: https://pubs.acs.org/10.1021/acssensors.5c01225

Author Contributions

J.B.L.: Conceptualization, methodology, writing—review and editing. E.R.: Methodology, review and editing. M.K.: Methodology, review and editing. S.H.: Methodology. S.K.: Methodology. E.C.: Methodology, review and editing. S.A.M.: Writing—review and editing. S.J.: Supervision, project administration, funding acquisition. Y.S.J.: Supervision, project administration, funding acquisition. Y.N.: Conceptualization, methodology, writing—review and editing, supervision, project administration, funding acquisition.

Notes

The authors declare no competing financial interest.

https://doi.org/10.1021/acssensors.5c01225
ACS Sens. 2025, 10, 5908−5917

■ ACKNOWLEDGMENTS

This work was supported by the Basic Science Research Program (RS-2025-00516761) and National R&D Program (2022M3H4A1A01012816) through the National Research Foundation of Korea (NRF) grant funded by the Ministry of Science and ICT (MSIT). We acknowledge funding and support from e-conversion German Cluster of Excellence from the DFG (German Research Foundation) under Germany's Excellence Strategy—EXC 2089/1-390776260, the Bavarian program Solar Technologies Go Hybrid (SolTech), the Center for NanoScience (CeNS), and the European Commission through the ERC Starting Grant CATALIGHT (802989). S.A.M. additionally acknowledges the Lee-Lucas Chair in Physics.

■ REFERENCES

(1) Chen, J.; Andler, S. M.; Goddard, J. M.; Nugen, S. R.; Rotello, V. M. Integrating Recognition Elements with Nanomaterials for Bacteria Sensing. *Chem. Soc. Rev.* **2017**, *46* (5), 1272−1283.

(2) Wu, X.; Xu, C.; Tripp, R. A.; Huang, Y. W.; Zhao, Y. Detection and differentiation of foodborne pathogenic bacteria in mung bean sprouts using field deployable label-free SERS devices. *Analyst* **2013**, *138* (10), 3005−3012.

(3) Wang, P.; Sun, Y.; Li, X.; Wang, L.; Xu, Y.; He, L.; Li, G. Recent advances in dual recognition based surface enhanced Raman scattering for pathogenic bacteria detection: A review. *Anal. Chim. Acta* **2021**, *1157*, No. 338279.

(4) Rajapaksha, P.; Elbourne, A.; Gangadoo, S.; Brown, R.; Cozzolino, D.; Chapman, J. A Review of Methods for the Detection of Pathogenic Microorganisms. *Analyst* **2019**, *144* (2), 396−411.

(5) Zeng, R.; Zhou, F.; Wang, Y.; Liao, Z.; Qian, S.; Luo, Q.; Zheng, J. Polydopamine modified colloidal gold nanotag-based lateral flow immunoassay platform for highly sensitive detection of pathogenic bacteria and fast evaluation of antibacterial agents. *Talanta* **2024**, *278*, No. 126525.

(6) Cheng, W.; Shi, H.; Teng, M.; Yu, M.; Feng, B.; Ding, C.; Yu, S.; Yang, F. Rapid identification of bacterial mixtures in urine using MALDI-TOF MS-based algorithm profiling coupled with magnetic enrichment. *Analyst* **2022**, *147* (3), 443−449.

(7) Novakovic, Z.; Khalife, M.; Costache, V.; Camacho, M. J.; Cardoso, S.; Martins, V.; Gadjanski, I.; Radovic, M.; Vidic, J. Rapid Detection and Identification of Vancomycin-Sensitive Bacteria Using an Electrochemical Apta-Sensor. *ACS Omega* **2024**, *9* (2), 2841−2849.

(8) Bravo-Frank, N.; Zende, R.; Feng, L.; Mesyngier, N.; Pachpute, A.; Hong, J. Realtime bacteria detection and analysis in sterile liquid products using deep learning holographic imaging. *npj Biosens.* **2024**, *1* (1), 8.

(9) Zhou, X.; Hu, Z.; Yang, D.; Xie, S.; Jiang, Z.; Niessner, R.; Haisch, C.; Zhou, H.; Sun, P. Bacteria Detection: From Powerful SERS to Its Advanced Compatible Techniques. *Adv. Sci.* **2020**, *7* (23), 2001739.

(10) Wang, Y.; Zhang, Z.; Sun, Y.; Wu, H.; Luo, L.; Song, Y. Recent Advances in Surface-Enhanced Raman Scattering for Pathogenic Bacteria Detection: A Review. *Sensors* **2025**, *25* (5), 1370.

(11) Zhou, H.; Yang, D.; Ivleva, N. P.; Mircescu, N. E.; Niessner, R.; Haisch, C. SERS detection of bacteria in water by in situ coating with Ag nanoparticles. *Anal. Chem.* **2014**, *86* (3), 1525−1533.

(12) Dina, N. E.; Zhou, H.; Colnita, A.; Leopold, N.; Szoke-Nagy, T.; Coman, C.; Haisch, C. Rapid single-cell detection and identification of pathogens by using surface-enhanced Raman spectroscopy. *Analyst* **2017**, *142* (10), 1782−1789.

(13) Tadesse, L. F.; Ho, C. S.; Chen, D. H.; Arami, H.; Banaei, N.; Gambhir, S. S.; Jeffrey, S. S.; Saleh, A. A. E.; Dionne, J. Plasmonic and Electrostatic Interactions Enable Uniformly Enhanced Liquid Bacterial Surface-Enhanced Raman Scattering (SERS). *Nano Lett.* **2020**, *20* (10), 7655−7661.

(14) Safir, F.; Vu, N.; Tadesse, L. F.; Firouzi, K.; Banaei, N.; Jeffrey, S. S.; Saleh, A. A. E.; Khuri-Yakub, B. P. T.; Dionne, J. A. Combining Acoustic Bioprinting with AI-Assisted Raman Spectroscopy for High-Throughput Identification of Bacteria in Blood. *Nano Lett.* **2023**, *23* (6), 2065−2073.

(15) Segervald, J.; Malyshev, D.; Oberg, R.; Zall, E.; Jia, X.; Wagberg, T.; Andersson, M. Ultra-Sensitive Detection of Bacterial Spores via SERS. *ACS Sens* **2025**, *10* (2), 1237−1248.

(16) Park, S.; Kim, K.; Go, A.; Lee, M. H.; Chen, L.; Choo, J. Rapid and Sensitive Escherichia coli Detection: Integration of SERS and Acoustofluidics in a Lysis-Free Microfluidic Platform. *ACS Sens* **2025**, *10* (2), 1217−1227.

(17) Liu, T. Y.; Tsai, K. T.; Wang, H. H.; Chen, Y.; Chen, Y. H.; Chao, Y. C.; Chang, H. H.; Lin, C. H.; Wang, J. K.; Wang, Y. L. Functionalized arrays of Raman-enhancing nanoparticles for capture and culture-free analysis of bacteria in human blood. *Nat. Commun.* **2011**, *2*, 538.

(18) Witkowska, E.; Nicinski, K.; Korsak, D.; Szymborski, T.; Kaminska, A. Sources of variability in SERS spectra of bacteria: comprehensive analysis of interactions between selected bacteria and plasmonic nanostructures. *Anal. Bioanal. Chem.* **2019**, *411* (10), 2001−2017.

(19) Andrei, C. C.; Moraillon, A.; Larquet, E.; Potara, M.; Astilean, S.; Jakab, E.; Bouckaert, J.; Rosselle, L.; Skandrani, N.; Boukherroub, R.; et al. SERS characterization of aggregated and isolated bacteria deposited on silver-based substrates. *Anal. Bioanal. Chem.* **2021**, *413* (5), 1417−1428.

(20) Senapati, S.; Kaur, M.; Singh, N.; Kulkarni, S. S.; Singh, J. P. Affordable Paper-Based Surface-Enhanced Raman Scattering Substrates Containing Silver Nanorods Using Glancing-Angle Deposition for Nosocomial Infection Detection. *ACS Applied Nano Materials* **2024**, *7* (7), 6736−6748.

(21) Zhou, H.; Yang, D.; Ivleva, N. P.; Mircescu, N. E.; Schubert, S.; Niessner, R.; Wieser, A.; Haisch, C. Label-Free in Situ Discrimination of Live and Dead Bacteria by Surface-Enhanced Raman Scattering. *Anal. Chem.* **2015**, *87* (13), 6553−6561.

(22) Sengupta, A.; Mujacic, M.; Davis, E. J. Detection of Bacteria by Surface-Enhanced Raman Spectroscopy. *Anal. Bioanal. Chem.* **2006**, *386* (5), 1379−1386.

(23) Kahraman, M.; Yazici, M. M.; Sahin, F.; Culha, M. Convective Assembly of Bacteria for Surface-Enhanced Raman Scattering. *Langmuir* **2008**, *24*, 894−901.

(24) Barton, S. J.; O'Dwyer, K.; Butler, M.; Dignam, A.; Byrne, H. J.; O'Neill, L.; Hennelly, B. M. Improved performance of near infrared excitation Raman spectroscopy using reflective thin-film gold on glass substrates for cytology samples. *Anal. Methods* **2019**, *11* (47), 6023−6032.

(25) Malaquin, L.; Kraus, T.; Schmid, H.; Delamarche, E.; Wolf, H. Controlled Particle Placement through Convective and Capillary Assembly. *Langmuir* **2007**, *23*, 11513−11521.

(26) Henzie, J.; Andrews, S. C.; Ling, X. Y.; Li, Z.; Yang, P. Oriented Assembly of Polyhedral Plasmonic Nanoparticle Clusters. *Proc. Natl. Acad. Sci. U.S.A.* **2013**, *110* (17), 6640−6645.

(27) Ni, S.; Leemann, J.; Wolf, H.; Isa, L. Insights into Mechanisms of Capillary Assembly. *Faraday Discuss.* **2015**, *181*, 225−242.

(28) Ni, S.; Leemann, J.; Buttinoni, I.; Isa, L.; Wolf, H. Programmable Colloidal Molecules from Sequential Capillarity-Assisted Particle Assembly. *Sci. Adv.* **2016**, *2*, No. e1501779.

(29) Scarabelli, L.; Vila-Liarte, D.; Mihi, A.; Liz-Marzán, L. M. Templated Colloidal Self-Assembly for Lattice Plasmon Engineering. *Acc. Chem. Res.* **2021**, *2* (9), 816−827.

(30) Redolat, J.; Camarena-Perez, M.; Griol, A.; Kovylina, M.; Xomalis, A.; Baumberg, J. J.; Martinez, A.; Pinilla-Cienfuegos, E. Accurate Transfer of Individual Nanoparticles onto Single Photonic Nanostructures. *ACS Appl. Mater. Interfaces* **2023**, *15* (2), 3558−3565.

(31) Urban, A. S.; Lutich, A. A.; Stefani, F. D.; Feldmann, J. Laser Printing Single Gold Nanoparticles. *Nano Lett.* **2010**, *10* (12), 4794−4798.

https://doi.org/10.1021/acssensors.5c01225
ACS Sens. 2025, 10, 5908−5917

(32) Gargiulo, J.; Violi, I. L.; Cerrota, S.; Chvátal, L.; Cortés, E.; Perassi, E. M.; Diaz, F.; Zemánek, P.; Stefani, F. D. Accuracy and Mechanistic Details of Optical Printing of Single Au and Ag Nanoparticles. *ACS Nano* **2017**, *11* (10), 9678−9688.
(33) Giersig, M.; Mulvaney, P. Preparation of Ordered Colloid Monolayers by Electrophoretic Deposition. *Langmuir* **1993**, *9*, 3408−3413.
(34) Zhang, H.; Cadusch, J.; Kinnear, C.; James, T.; Roberts, A.; Mulvaney, P. Direct Assembly of Large Area Nanoparticle Arrays. *ACS Nano* **2018**, *12* (8), 7529−7537.
(35) Charlot, B.; Bardin, F.; Sanchez, N.; Roux, P.; Teixeira, S.; Schwob, E. Elongated Unique DNA Strand Deposition on Micro-structured Substrate by Receding Meniscus Assembly and Capillary Force. *Biomicrofluidics* **2014**, *8* (1), No. 014103.
(36) Cayron, H.; Berteloite, B.; Vieu, C.; Paveau, V.; Cau, J.-C.; Cerf, A. Controlled Deposition and Multi-Layer Architecturing of Single Biomolecules Using Automated Directed Capillary Assembly and Nano-Contact Printing Processes. *Microelectron. Eng.* **2015**, *135*, 1−6.
(37) Diguet, A.; Le Berre, M.; Chen, Y.; Baigl, D. Preparation of Phospholipid Multilayer Patterns of Controlled Size and Thickness by Capillary Assembly on a Microstructured Substrate. *Small* **2009**, *5* (14), 1661−1666.
(38) Formosa, C.; Pillet, F.; Schiavone, M.; Duval, R. E.; Ressier, L.; Dague, E. Generation of Living Cell Arrays for Atomic Force Microscopy Studies. *Nat. Protoc.* **2015**, *10* (1), 199−204.
(39) Pioli, R.; Stocker, R.; Isa, L.; Secchi, E. Patterning of Microorganisms and Microparticles through Sequential Capillarity-assisted Assembly. *J. Vis. Exp.* **2021**, *177*, No. e63131.
(40) Butler, H. J.; Ashton, L.; Bird, B.; Cinque, G.; Curtis, K.; Dorney, J.; Esmonde-White, K.; Fullwood, N. J.; Gardner, B.; Martin-Hirsch, P. L.; et al. Using Raman spectroscopy to characterize biological materials. *Nat. Protoc.* **2016**, *11* (4), 664−687.
(41) Kerr, L. T.; Byrne, H. J.; Hennelly, B. M. Optimal Choice of Sample Substrate and Laser Wavelength for Raman Spectroscopic Analysis of Biological Specimen. *Anal. Methods* **2015**, *7* (12), 5041−5052.
(42) Mosier-Boss, P. A. Review on SERS of Bacteria. *Biosensors* **2017**, *7*, 51.
(43) Liu, T. T.; Lin, Y. H.; Hung, C. S.; Liu, T. J.; Chen, Y.; Huang, Y. C.; Tsai, T. H.; Wang, H. H.; Wang, D. W.; Wang, J. K.; et al. A high speed detection platform based on surface-enhanced Raman scattering for monitoring antibiotic-induced chemical changes in bacteria cell wall. *PLoS One* **2009**, *4* (5), No. e5470.
(44) Premasiri, W. R.; Gebregziabher, Y.; Ziegler, L. D. On the Difference between Surface-Enhanced Raman Scattering (SERS) Spectra of Cell Growth Media and Whole Bacterial Cells. *Appl. Spectrosc.* **2011**, *65* (5), 493−499.
(45) Barzan, G.; Sacco, A.; Mandrile, L.; Giovannozzi, A. M.; Portesi, C.; Rossi, A. M. Hyperspectral Chemical Imaging of Single Bacterial Cell Structure by Raman Spectroscopy and Machine Learning. *Appl. Sci.* **2021**, *11* (8), 3409.
(46) Jo, Y.; Jung, J.; Lee, J. W.; Shin, D.; Park, H.; Nam, K. T.; Park, J. H.; Park, Y. Angle-resolved light scattering of individual rod-shaped bacteria based on Fourier transform light scattering. *Sci. Rep.* **2014**, *4*, 5090.
(47) Oh, Y.-J.; Kang, M.; Park, M.; Jeong, K.-H. Engineering Hot Spots on Plasmonic Nanopillar Arrays for SERS: A Review. *BioChip J.* **2016**, *10* (4), 297−309.
(48) Lee, S.; Choi, I. Fabrication Strategies of 3D Plasmonic Structures for SERS. *BioChip J.* **2019**, *13* (1), 30−42.
(49) Araujo, G. R. S.; Viana, N. B.; Gomez, F.; Pontes, B.; Frases, S. The Mechanical Properties of Microbial Surfaces and Biofilms. *Cell Surf.* **2019**, *5*, No. 100028.
(50) LeCun, Y.; Bengio, Y.; Hinton, G. Deep Learning. *Nature* **2015**, *521* (7553), 436−444.
(51) He, K.; Zhang, X.; Ren, S.; Sun, J. Deep Residual Learning for Image Recognition. In *2016 IEEE Conference on Computer Vision and Pattern Recognition (CVPR)*, 2016; pp. 770−778.
(52) Guo, Y.; Liu, Y.; Oerlemans, A.; Lao, S.; Wu, S.; Lew, M. S. Deep Learning for Visual Understanding: A Review. *Neurocomputing* **2016**, *187*, 27−48.
(53) Fan, X.; Ming, W.; Zeng, H.; Zhang, Z.; Lu, H. Deep Learning-Based Component Identification for the Raman Spectra of Mixtures. *Analyst* **2019**, *144* (5), 1789−1798.
(54) Ho, C. S.; Jean, N.; Hogan, C. A.; Blackmon, L.; Jeffrey, S. S.; Holodniy, M.; Banaei, N.; Saleh, A. A. E.; Ermon, S.; Dionne, J. Rapid Identification of Pathogenic Bacteria using Raman Spectroscopy and Deep Learning. *Nat. Commun.* **2019**, *10* (1), 4927.
(55) Rho, E.; Kim, M.; Cho, S. H.; Choi, B.; Park, H.; Jang, H.; Jung, Y. S.; Jo, S. Separation-Free Bacterial Identification in Arbitrary Media via Deep Neural Network-based SERS Analysis. *Biosens. Bioelectron.* **2022**, *202*, No. 113991.
(56) Kang, H.; Lee, J.; Moon, J.; Lee, T.; Kim, J.; Jeong, Y.; Lim, E. K.; Jung, J.; Jung, Y.; Lee, S. J.; et al. Multiplex Detection of Foodborne Pathogens using 3D Nanostructure Swab and Deep Learning-Based Classification of Raman Spectra. *Small* **2024**, *20* (35), No. e2308317.
(57) Sacco, A.; Botto, C. S.; D'Errico, C.; Ciuffo, M.; Matić, S.; Molinatto, G.; Giovannozzi, A. M.; Rossi, A. M.; Noris, E. Characterization of plant pathogenic bacteria at subspecies level using a dielectrophoresis device combined with Raman spectroscopy. *Biosens. Bioelectron.: X* **2025**, *23*, No. 100595.
(58) Lee, J. B.; Walker, H.; Li, Y.; Nam, T. W.; Rakovich, A.; Sapienza, R.; Jung, Y. S.; Nam, Y. S.; Maier, S. A.; Cortes, E. Template Dissolution Interfacial Patterning of Single Colloids for Nano-electrochemistry and Nanosensing. *ACS Nano* **2020**, *14* (12), 17693−17703.
(59) Chen, T.; Reinhard, B. M. Assembling Color on the Nanoscale: Multichromatic Switchable Pixels from Plasmonic Atoms and Molecules. *Adv. Mater.* **2016**, *28* (18), 3522−3527.
(60) Premasiri, W. R.; Chen, Y.; Williamson, P. M.; Bandarage, D. C.; Pyles, C.; Ziegler, L. D. Rapid urinary tract infection diagnostics by surface-enhanced Raman spectroscopy (SERS): identification and antibiotic susceptibilities. *Anal. Bioanal. Chem.* **2017**, *409* (11), 3043−3054.
(61) Tien, N.; Lin, T. H.; Hung, Z. C.; Lin, H. S.; Wang, I. K.; Chen, H. C.; Chang, C. T. Diagnosis of Bacterial Pathogens in the Urine of Urinary-Tract-Infection Patients Using Surface-Enhanced Raman Spectroscopy. *Molecules* **2018**, *23* (12), 3374.
(62) Lee, J.-C.; Kim, J.-O.; Lee, H.-J.; Shin, B.; Park, S. Meniscus-Guided Control of Supersaturation for the Crystallization of High Quality Metal Organic Framework Thin Films. *Chem. Mater.* **2019**, *31* (18), 7377−7385.
(63) Paszke, A.; Gross, S.; Massa, F.; Lerer, A.; Bradbury, J.; Chanan, G.; Trevor Killeen, T.; Zeming Lin, Z.; Natalia Gimelshein, N.; Luca Antiga, L.et al.PyTorch: An Imperative Style, High-Performance Deep Learning Library. In *NeurIPS 2019*; Wallach, H.; Larochelle, H.; Beygelzimer, A.; d'Alché-Buc, F.; Fox, E.; Garnett, R., Eds., 2019.
(64) Loshchilov, I.; Hutter, F. Decoupled Weight Decay Regularization. In *ICLR 2019*, 2019.

https://doi.org/10.1021/acssensors.5c01225
ACS Sens. 2025, 10, 5908−5917